Available online at www.sciencedirect.com
ScienceDirect
C. R. Mecanique 334 (2006) 507–516
COMPTES RENDUS MECANIQUE
http://france.elsevier.com/direct/CRAS2B/

Observation, analysis and modelling in complex fluid media

Comparison of transported scalar PDF and velocity-scalar PDF approaches to 'Delft flame III'

Dirk Roekaerts [a,*], Bart Merci [b], Bertrand Naud [c]

[a] *Department of Multi-Scale Physics, Delft University of Technology, Lorentzweg 1, NL-2628 CJ Delft, The Netherlands*
[b] *Department of Flow, Heat and Combustion Mechanics, Ghent University – UGent, B-9000 Ghent, Belgium*
[c] *CIEMAT, Avda. Complutense, 22, 28040 Madrid, Spain*

Abstract

Numerical simulation results are presented for the turbulent piloted jet diffusion flame 'Delft Flame III'. In this flame, which is one of the target flames of the International Workshop on Measurements and Computations of Turbulent Nonpremixed Flames (TNF), effects of turbulence-chemistry interaction are strong and modelling the turbulence-chemistry interaction is a challenge. After an outline of the theoretical framework, a comparison is presented of results with on the one hand the velocity-scalar transported probability density function (PDF) approach with reduced chemistry (ILDM) and on the other hand the scalar PDF approach with detailed chemistry (C_1-mechanism). The same micromixing model (modified coalescence-dispersion model, CD) is used in both studies. The reasons for the significantly better prediction of the mean temperature field by the scalar PDF calculations are discussed. Results of other micromixing models are briefly mentioned. ***To cite this article: D. Roekaerts et al., C. R. Mecanique 334 (2006).***

Résumé

Comparaison des approches basées sur la PDF d'un scalaire transporté et sur la PDF jointe vitesse-scalaire appliquées à la flamme « Delft III ». Des résultats de simulation numérique sont présentés pour la flamme de diffusion pilotée « Delft III ». Dans cette flamme, qui constitue l'un des cas tests pour le International Workshop on Measurements and Computations of Turbulent Nonpremixed Flames (TNF), les effets de l'interaction entre la turbulence et les processus liés à la chimie sont forts et la modélisation de ces interactions constitue donc un challenge. Après avoir exposé le contexte théorique, nous présenterons la comparaison des résultats obtenus avec d'une part une approche basée sur l'équation d'évolution de la densité de probabilité (PDF) jointe vitesse-scalaire associée à un schéma chimique réduit (ILDM) et d'autre part une approche basée sur la PDF du scalaire associée à un schéma chimique détaillé (mécanisme C_1). Le même modèle de micro-mélange (modèle modifié de dispersion-coalescence, CD) est utilisé dans les deux approches. Les raisons qui conduisent à une amélioration considérable du champ de température moyenne lorsque l'on effectue des calculs basés sur la PDF du scalaire sont discutées. Les résultats obtenus avec d'autres modèles de micro-mélange sont brièvement mentionnés. ***Pour citer cet article : D. Roekaerts et al., C. R. Mecanique 334 (2006).***

Keywords: Turbulence; Combustion; Turbulent combustion modeling; Micromixing; Probability density functions

Mots-clés : Turbulence ; Combustion ; Modèles de combustion turbulente ; Micro-mélange ; Densités de probabilité

* Corresponding author.
E-mail addresses: d.j.e.m.roekaerts@tudelft.nl (D. Roekaerts), bart.merci@ugent.be (B. Merci), bertrand.naud@ciemat.es (B. Naud).

1631-0721/$ – see front matter
doi:10.1016/j.crme.2006.07.007

1. Introduction

The micromixing term in the one-point PDF transport equations describes the transport of probability in composition space by molecular fluxes [1–4]. It is an unclosed term because it depends on multi-point information, in particular information on the spatial gradients. Many models have been proposed to close the micromixing term, and for discussion of recent developments we refer the reader to [4,5]. The introduction and testing of new models usually have been done by considering simple test cases such as the decay of a passive scalar in homogeneous, isotropic turbulence. These test cases allow for the study of the interaction between micromixing and chemical reaction as a function of an externally imposed mixing frequency. However, if the models are to be used in actual turbulent flame calculations, it is necessary to have insight in their performance under these conditions. Accordingly studies have appeared in the literature where two or more micromixing models are applied to experimentally well-documented flames and the dependence of the quality of the predictions is related to the properties of the micromixing models. In particular such study has been made by Nooren et al. [5,6] for the case of 'Delft Flame III' [7–9], one of the target flames of the International Workshop on Measurement and Computation of Turbulent Nonpremixed Flames [10].

The burner head of the Delft burner is schematically shown in Fig. 1. The fuel jet, emerging from the central pipe, is surrounded by primary air through the annulus. Specific features are a constriction of the fuel pipe (from 8 to 6 mm diameter) upstream of the nozzle exit, as well as the conical shape of the interior of the primary air annulus. The fuel is Dutch natural gas, simplified in the simulations as 85.3% methane and 14.7% nitrogen (by volume). The stoichiometric mixture fraction is $\xi_{st} = 0.07$.

The Reynolds number, based on mean fuel velocity and diameter (6 mm), is 9700. Around the fuel, the primary air emerges from the annulus with mean velocity equal to 4.5 m/s. Around the primary air annulus, a co-flow air stream ($U = 0.4$ m/s) exists. The flame is stabilized through pilot flames, issued from 12 holes (diameter 0.5 mm), in between the fuel and the primary air annulus. The turbulence-chemistry interaction in this flame is sufficiently strong to have local extinction phenomena and it provides a challenging test case for turbulent combustion models and for micromixing models in particular.

Nooren et al. [5,6] calculated Flame III using the hybrid finite volume/joint velocity-scalar transported PDF method. Firstly a fast chemistry model was used in combination with three micromixing models: Interaction by Ex-

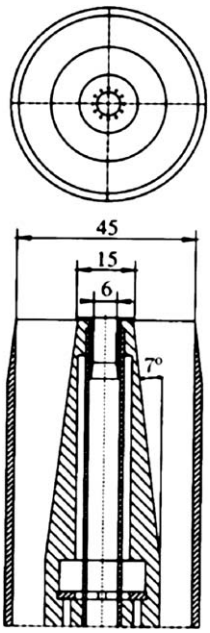

Fig. 1. Drawing of the burner head of the Delft turbulent diffusion flame burner. Distances are indicated in mm.

Fig. 1. Schéma de la tête du brûleur utilisé à Delft. Les distances sont en mm.

change with the Mean (IEM), a Coalescence-Dispersion model (CD-model, also known as modified Curl model) and the Mapping Closure Model (MCM). Comparisons between experiments and computations were made for mixture fraction PDF and for mean and standard deviation of temperature. It was concluded that relatively small differences in the mixture fraction PDF can have appreciable effects on the resulting temperature field. It was found that the IEM model does not mimic the experimental profile of standard deviation of temperature (radial profiles) as closely as the other two micromixing models. Subsequently, effects of finite rate chemistry were studied, using a reduced chemistry model employing an Intrinsic Low-Dimensional Manifold (ILDM) with two reacting scalars. These calculations were done using the CD model. To obtain an attached flame, the value of the model constant C_ϕ had to be set to 4, rather than the default value 2. The IEM was not used because of the worse performance in the first part of the study and the MCM was not used because, barring exceptions, this model is limited to cases with one reacting scalar. Using finite rate chemistry local extinction could be taken into account and reasonable joint probability density functions of mixture fraction and temperature or of mixture fraction and some chemical components could be obtained (such joint PDF's are represented as scatter plots, see below). However, the amount of local extinction was still underpredicted and the agreement between model and experiments was still far from perfect. The question arises whether better agreement can be obtained by improvements in turbulence modelling, micromixing modelling or by incorporating more detailed chemistry, or by a combination of them.

In a recent study by Merci et al. [11,12] new results for Delft Flame III were obtained using a transported scalar PDF method. Detailed chemistry has been employed, using In-Situ Adaptive Tabulation (ISAT) to keep the computational effort manageable. The flow fields and mixing fields were studied in [11], the relative performance of micromixing models was studied in [12]. In [12] it was reported that with the IEM model, global extinction occurs. With the 'standard' value of model constant $C_\phi = 2$, the CD model yields a lifted flame, unlike the experiments, while with the EMST model the correct flame shape is obtained. However, the conditional variances of the thermo-chemical quantities are under-estimated with the EMST model, due to a lack of local extinction in the simulations. With the CD model, the flame becomes attached when either the value of C_ϕ is increased to 3 or the pilot flame thermal power is increased by a factor 1.5. With increased value of C_ϕ better results for mixture fraction variance are obtained, both with the CD and the EMST model. Lowering the value of C_ϕ leads to better predictions for mean temperature with EMST, but at the cost of worse over-prediction of mixture fraction variance.

In Delft Flame III, the pilot flames emerge from 12 separate holes. However, the simulations are performed in a plane, under the assumption of axisymmetry. Therefore, special care must be taken for the treatment of the pilot flames. For calculations using equilibrium chemistry, the pilot flames can simply be omitted. They are not necessary since when equilibrium chemistry is applied ignition automatically occurs after mixing. Furthermore, the mass flow rate of the pilot flames is small, so that the error in the flow field is small when they are omitted. For the transported PDF simulations with finite rate chemistry, however, the flame no longer ignites when the pilot flames are omitted. In order to avoid a flow field error due to an unrealistic axisymmetric representation of the flow through the 12 holes, the influence of the pilot flame is taken into account by an influence on the local thermodynamic conditions in a region inside the computational domain close to the burner rim. A first method, applied in [6,7], is to force the flame to ignite in this 'pilot flame zone' by transforming all particles in the pilot flame zone to flame sheet (mixed-is-burnt) conditions. The size of the pilot flame zone was defined by $x < 35$ mm, $0\ \text{mm} < r < 15$ mm. A second method, introduced in [11] and also used in [12], is to add a volumetric energy source, corresponding to the thermal power of the pilot flames (around 200 W), in a smaller pilot flame zone ($x < 20$ mm, $4\ \text{mm} < r < 7$ mm).

In this work we make a detailed comparison of the calculations of [6,7] and [12], both using CD model and predicting an attached flame. This analysis demonstrates the difficulty to evaluate the performance of the submodel for micromixing model in a real flame where the visibility of the error of a micromixing model may be small due to the dominant role of other submodels.

2. One-point PDF modeling

The dynamical evolution of the Newtonian fluid turbulent flow considered is given by the continuity equation, the Navier–Stokes equations, the conservation equations for N species mass fractions and for specific enthalpy. The low Mach number approximation is used. The vector of scalar variables then contains $N + 1$ components, the species mass fractions and the specific enthalpy. By simplifying assumptions the number of independent scalar variables can be reduced. The independent scalar variables will also be called 'composition variables'. The temperature is obtained

from the caloric equation of state. The density is related to composition and pressure via the ideal gas equation of state.

The statistical description of the flow is made in terms of the one-point joint PDF of velocity and composition $f_{U\phi}$, such that that $f_{U\phi}(\boldsymbol{V},\psi;\boldsymbol{x},t)\,\mathrm{d}\boldsymbol{V}\,\mathrm{d}\psi$ is the probability that velocity is in the interval $[\boldsymbol{V},\boldsymbol{V}+\mathrm{d}\boldsymbol{V}]$ and scalar variables are in the interval $[\psi,\psi+\mathrm{d}\psi]$ at $(\boldsymbol{x},t)$.

The PDF $f_{U\phi}$ defines mean values (or expected values) as [13]:

$$\big\langle Q(\boldsymbol{x},t)\big\rangle = \int\limits_{[\boldsymbol{V},\psi]} \langle Q \mid \boldsymbol{V},\psi\rangle f_{U\phi}(\boldsymbol{V},\psi;\boldsymbol{x},t)\,\mathrm{d}\boldsymbol{V}\,\mathrm{d}\psi \tag{1}$$

Fluctuations are defined as: $q'(\boldsymbol{x},t) = Q(\boldsymbol{x},t) - \langle Q(\boldsymbol{x},t)\rangle$.

For variable density flows, it is useful to consider the joint mass density function (MDF) $F_{U\phi}(\boldsymbol{V},\psi) = \rho(\psi) f_{U\phi}(\boldsymbol{V},\psi)$. Density weighted averages (Favre averages) can be considered:

$$\widetilde{Q}(\boldsymbol{x},t) = \frac{\langle \rho(\boldsymbol{x},t) Q(\boldsymbol{x},t)\rangle}{\langle \rho(\boldsymbol{x},t)\rangle} = \frac{\int_{[\boldsymbol{V},\psi]} \langle Q \mid \boldsymbol{V},\psi\rangle F_{U\phi}(\boldsymbol{V},\psi;\boldsymbol{x},t)\,\mathrm{d}\boldsymbol{V}\,\mathrm{d}\psi}{\int_{[\boldsymbol{V},\psi]} F_{U\phi}(\boldsymbol{V},\psi;\boldsymbol{x},t)\,\mathrm{d}\boldsymbol{V}\,\mathrm{d}\psi} \tag{2}$$

Fluctuations with respect to the Favre average are defined as: $q''(\boldsymbol{x},t) = Q(\boldsymbol{x},t) - \widetilde{Q}(\boldsymbol{x},t)$.

Using the Navier–Stokes equations and the scalar transport equations, the MDF transport equation can be expressed as:

$$\begin{aligned}
&\frac{\partial F_{U\phi}}{\partial t} + V_j \frac{\partial F_{U\phi}}{\partial x_j} + \left(-\frac{1}{\rho(\psi)}\frac{\partial\langle p\rangle}{\partial x_i} + \frac{1}{\rho(\psi)}\frac{\partial\langle\tau_{ij}\rangle}{\partial x_j} + g_i\right)\frac{\partial F_{U\phi}}{\partial V_i} + \frac{\partial}{\partial\psi}S(\psi)F_{U\phi} \\
&\quad = -\frac{\partial}{\partial V_i}\left[\frac{1}{\rho(\psi)}\left\langle -\frac{\partial p'}{\partial x_i} + \frac{\partial\tau'_{ij}}{\partial x_j} \;\middle|\; \boldsymbol{V},\psi\right\rangle F_{U\phi}\right] - \frac{\partial}{\partial\psi}\left[\frac{1}{\rho(\psi)}\left\langle -\frac{\partial J_j}{\partial x_j} \;\middle|\; \boldsymbol{V},\psi\right\rangle F_{U\phi}\right]
\end{aligned} \tag{3}$$

The terms on the left-hand side of Eq. (3) appear in closed form: effects of convection, mean pressure gradient and chemical reaction are exactly accounted for. The mean viscous stress tensor gradient $\partial\langle\tau_{ij}\rangle/\partial x_j$ is neglected under the assumption of high Reynolds number. The chemical source term S is obtained from the chemistry mechanism. In [6,7] the chemical mechanism used is an evolution on an ILDM with three independent composition variables: mixture fraction and mass fractions of CO_2 and H_2O.

The terms on the right-hand side of Eq. (3), including the micromixing term depending on the conditional value of the gradient of the molecular flux, are not closed at the level of the MDF $F_{U\xi}$. This is due to the lack of information on time or length scale inherent to the one-point one-time statistical description. The missing information on turbulent scales is provided by a modelled dissipation of turbulent kinetic energy ε^M. A modelled transport equation for ε^M provides the closure.

The one-point joint PDF of composition can be obtained as the marginal PDF after integration of the velocity-scalar PDF over velocity space. Or equivalently, the joint Composition Mass Density Function (CMDF) is obtained by integration of the MDF.

$$F_\phi(\psi;\boldsymbol{x},t) = \int\limits_{[\boldsymbol{V}]} F_{U\phi}(\boldsymbol{V},\psi;\boldsymbol{x},t)\,\mathrm{d}\boldsymbol{V} \tag{4}$$

From the transport equation for the MDF the transport equation for the CMDF can be obtained. One has:

$$\frac{\partial F_\phi}{\partial t} + \widetilde{U}_j\frac{\partial F_\phi}{\partial x_j} + \frac{\partial}{\partial\psi}S(\psi)F_\phi = -\frac{1}{\bar\rho}\frac{\partial}{\partial x_i}\big[\bar\rho\langle u_i'' \mid \psi\rangle F_\phi\big] - \frac{\partial}{\partial\psi}\left[\frac{1}{\rho(\psi)}\left\langle -\frac{\partial J_j^\xi}{\partial x_j} \;\middle|\; \psi\right\rangle F_\phi\right] \tag{5}$$

The terms on the right-hand side of Eq. (5) are not closed at the level of the CMDF F_ϕ. The missing information is provided by a model for the turbulent transport and a model for the micromixing, which now in principle can depend on the properties calculated in the closure model for the velocity field. In [12] the two-equation nonlinear k–ε model of [14–16], containing an original transport equation for the turbulent dissipation rate is used. The chemical model used in [12] is the C_1 skeletal scheme of [17], containing 16 species and 41 reactions.

Because of the high dimensionality of $F_{U\phi}$, and F_ϕ it is not computationally efficient to solve a modelled equation for Eq. (3) or Eq. (5) by use of standard discretization methods. Instead, particle methods are used [1]. Modelling is therefore considered in a Lagrangian framework.

To solve Eq. (3), we consider a set of uniformly distributed computational particles evolving according to stochastic differential equations. Each particle has a set of properties $\{w^*, m^*, \boldsymbol{X}^*, \boldsymbol{U}^*, \phi^*\}$, where w^* is a numerical weight, m^* is the mass of the particle, $\boldsymbol{X}^*$ its position, $\boldsymbol{U}^*$ its velocity and ϕ^* the particle's scalar composition. The superscript * denotes that the quantity is a stochastic particle property. In addition to the listed properties it is of course possible to retrieve dependent properties such as density. A similar representation can be developed for the solution of Eq. (5), with particle velocity being absent from the list of particle properties.

The velocity-scalar method and the joint scalar PDF method differ in the way the influence of turbulent velocity fluctuations on the spatial transport of the particles is described. In the scalar PDF method it is done using a stochastic model for the displacement of particles, faithfully representing the model used for turbulent diffusivity [18]. (In [11, 12] the scalar PDF model has been combined with a nonlinear k–ε model [14–16].) In the joint velocity-scalar PDF method it is done by modelling the stochastic acceleration of the particle representing the PDF [19,13]. Hence, the two PDF models used differ in the representation of turbulent diffusivity. However, in [6,7] a hybrid finite volume/velocity-scalar PDF model has been used in which the Lagrangian model for particles is forced to agree with the mean velocity and turbulent kinetic energy predicted by a standard k–ε model with round jet correction. Consequently it is expected that differences between predictions of turbulent transport (Reynolds stress) between both approaches is due less to the PDF algorithm (velocity-scalar or scalar) than to the difference in k–ε model. On the other hand when it comes to the prediction of the Reynolds flux larger differences can arise.

The CD micromixing model prescribes the evolution of particle composition as a series of pair wise mixing events. The particles participating in mixing are chosen at random from the set of particles present in a finite volume cell and their compositions change in the direction of the partner. The degree of mixing in a pair is determined by a random variable uniformly distributed between 0 (no mixing) and 1 (complete mixing) [1,13].

3. Results

We now present and compare results obtained on the one hand by Nooren et al. [5,6] using the velocity-scalar PDF approach, k–ε model with round jet correction and ILDM and on the other hand by Merci et al. [12] using the scalar PDF approach, non-linear k–ε model and C_1-chemistry. (Out of the cases considered in [12] we mainly consider the case with pilot flame power 300 W and with $C_\phi = 2$.) In both cases a comparable size of computational domain, number of finite volume cells and number of particles per cell has been used. Also, both studies have been supported by a demonstration of grid independence (see [6,7] and [11,12] for details). Averaging over a number of iterations is performed in order to reduce statistical error in the mean fields. The analysis is restricted to results up to axial distance 150 mm. Results further downstream would not lead to different conclusions.

First the predictions of the velocity and turbulence field are considered.

Fig. 2 shows the radial profiles of mean axial velocity at two axial positions. It is confirmed that the standard k–ε model does not predict the spreading rate of the jet correctly. At axial distance 150 mm both the k–ε model with round jet correction (RJC) and the nonlinear k–ε model are in very good agreement with the measurements. At 50 mm the nonlinear k–ε model performs better. Fig. 3 shows the radial profiles of turbulent kinetic energy at the same axial positions. The nonlinear model slightly overpredicts the turbulent kinetic energy.

Next the mean mixing field and the prediction for mean temperature is considered. Fig. 4 shows the radial profile of mean mixture fraction and mean temperature at an axial distance of 100 mm. The bad prediction of the flow field by the standard k–ε model evidently also results in a bad prediction of the mixing field and will not be considered further. Both k–ε model with round jet correction and the nonlinear k–ε model predict the mean mixture fraction profile quite well but show a slight overprediction of the spreading rate. Correspondingly the location of the stoichiometric contour is positioned at too high radial position. However, there is a remarkable difference in the peak value of the mean temperature profile predicted by velocity-scalar PDF method using ILDM and the scalar PDF method using C_1-chemistry. Several possible explanations for this difference can be put forward. First we mention two features which do not provide an explanation. On the one hand, the difference in turbulence model does not seem to play a significant role. In the case of the application to the piloted jet diffusion flame having a relatively simple flow field the differences between the turbulence models used in [6,7] and [11,12] are expected to be small. On the

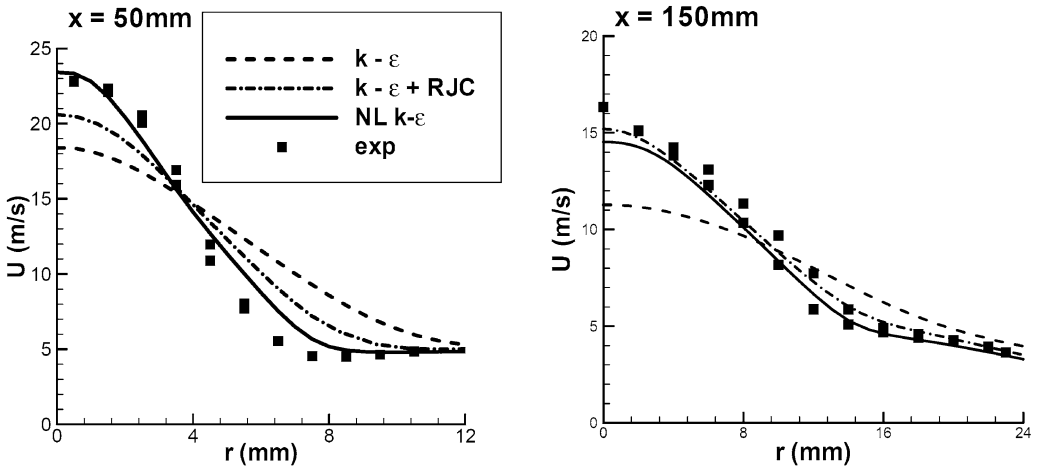

Fig. 2. Radial profiles of mean axial velocity at axial distances of 50 and 150 mm from the burner. Comparison of predictions with three different turbulence models. Experimental data from [20].

Fig. 2. Profils radiaux de la vitesse moyenne axiale aux distances axiales de 50 et 150 mm par rapport au brûleur. Comparaison des prédictions obtenues avec trois modèles différents de turbulence. Les données expérimentales sont celles publiées par [20].

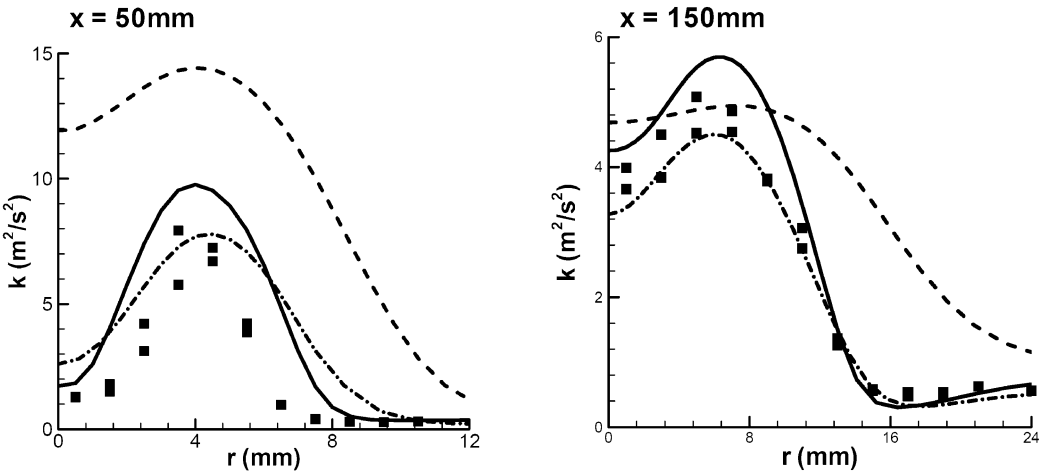

Fig. 3. Radial profiles of turbulent kinetic energy at axial distances of 50 and 150 mm from the burner. Comparison of predictions with three different turbulence models. Legend as in Fig. 2. Experimental data from [20].

Fig. 3. Profils radiaux de l'énergie cinétique de la turbulence aux distances axiales de 50 et 150 mm par rapport au brûleur. Comparaison des prédictions obtenues avec trois modèles différents de turbulence. Les données expérimentales sont celles publiées par [20]. Mêmes symboles que pour la Fig. 2.

other hand also a small difference in inlet profile between [6,7] and [11,12] was found to be unimportant (see [11] for full explanation). Other differences which seem to be important are: (i) different chemistry model; (ii) different model for the pilot flame; (iii) different value of model constant C_ϕ; and (iv) a different model for the Reynolds flux.

This will be investigated further by looking at the joint PDF of temperature and mixture fraction. This PDF can be represented in the form of a scatter plot. Fig. 5 shows the scatter plot belonging to the experimental data and the two model calculations. The represented points belong to the complete radial profile at height 100 mm above the burner. The effects of local extinction can be clearly seen in the large number of measurements with temperature lower than the burning flame conditions. Both PDF calculations show local extinction, but in the case of velocity-scalar PDF with ILDM there seems to be less local extinction than in the experiments. To make this statement quantitative it is

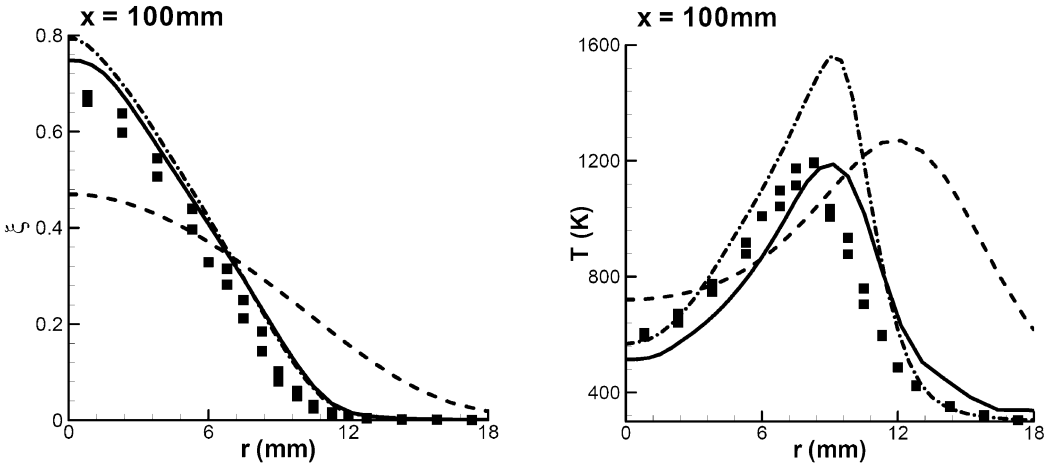

Fig. 4. Radial profiles of mean mixture fraction and mean temperature at axial distance 100 mm from the burner. Comparison of predictions of three different models. For turbulence model legend is as in Fig. 2. The k–ε with RJC was used with velocity-scalar PDF and ILDM. Nonlinear k–ε model was used with C_1-chemistry. CD micromixing was used in both cases.

Fig. 4. Profils radiaux de la fraction massique moyenne et de la température moyenne à la distance axiale de 100 mm par rapport au brûleur. Comparaison des prédictions obtenues avec trois modèles différents de turbulence. Mêmes symboles que pour la Fig. 2. Le modèle k–ε avec RJC a été utilisé avec la PDF vitesse-scalaire et le schéma ILDM pour la chimie. Le modèle k–ε non-linéaire a été utilisé avec la PDF vitesse-scalaire et le schéma C_1 pour la chimie. Le modèle CD de micro-mélange a été utilisé dans les deux cas.

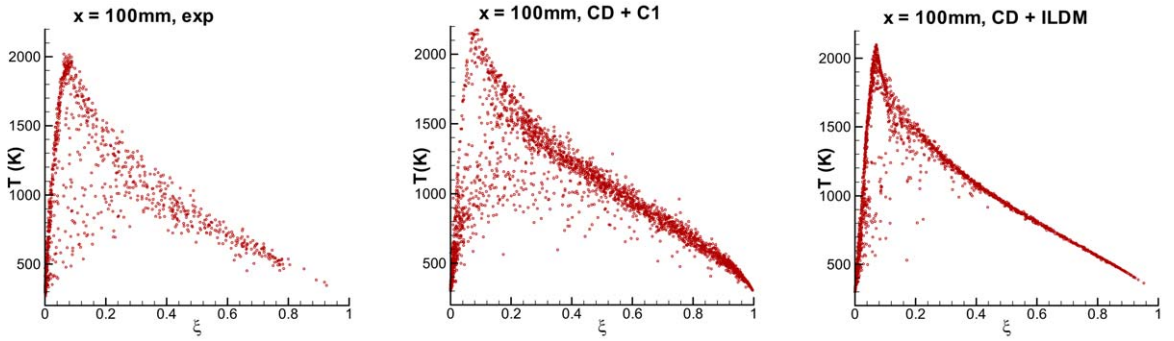

Fig. 5. Scatter plot of temperature versus mixture fraction axial distance 100 mm from the burner. Left: Experimental data from [8]. Middle: CD + C_1 model results by the method of [11,12] with pilot flame power 300 W and $C_\phi = 2$ (Fig. 9 in [12]). Right: CD + ILDM model results from [5,6] with $C_\phi = 4$.

Fig. 5. Données de température en fonction de la fraction massique obtenues à la distance axiale de 100 mm par rapport au brûleur. Gauche : Données expérimentales de [8]. Milieu : Résultats obtenus avec la méthode CD + C_1 présentée par [11,12] pour une puissance de flamme pilotée de 300 W et $C_\phi = 2$ (Fig. 9 de [12]). Droite : Résultats de la méthode CD + ILDM de [5,6] avec $C_\phi = 4$.

instructive to look at the conditional mean temperature. Fig. 6 (left) shows the conditional mean temperature belonging to the scatter plots of Fig. 5. It can be seen that both model calculations overpredict the conditional mean temperature at the rich side of the flame, but the overprediction is more severe for the scalar PDF method with C_1-chemistry. On the other hand, only the velocity-scalar PDF method with ILDM is able to reproduce correctly the conditional mean temperature at the lean side of the flame and in the stoichiometric zone. In that region the scalar PDF method with C_1-chemistry underpredicts conditional mean temperature.

We propose the following explanations: The pilot flame model used in combination with the velocity-scalar PDF and ILDM is relatively strong (all particles in the pilot flame zone are set to burnt conditions). The scatter plot seems to show that also at axial distance 100 mm the burnt state is overrepresented compared to experiments. On the other hand the scalar PDF method with C_1-chemistry was used in combination with a less drastic pilot flame model (heat was added to the mixture in the pilot flame zone). This procedure leaves it to the finite rate kinetics to bring the material to the burnt state. However, the first flammable material must be formed by the action of the micromix-

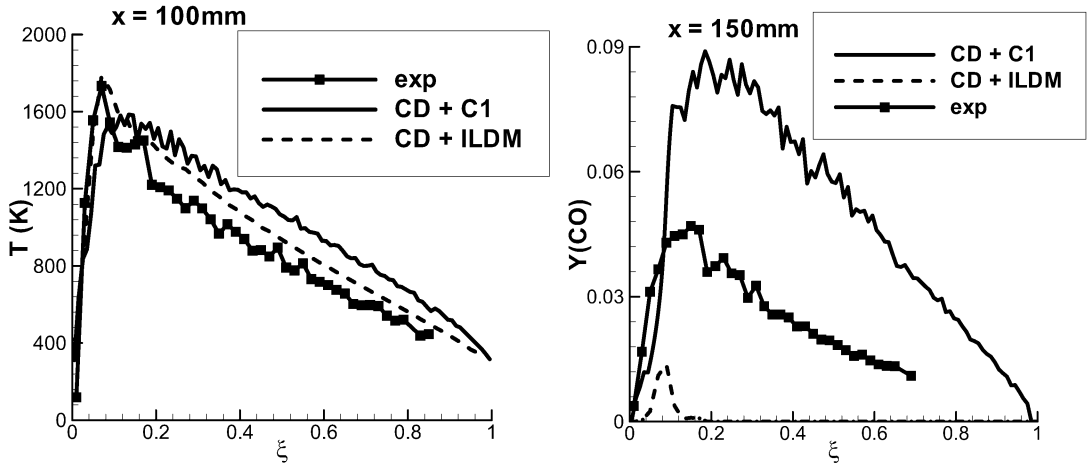

Fig. 6. Left: Profile of conditional mean temperature at axial distance 100 mm from the burner. Right: Profile of conditional mean CO mass fraction at axial distance 150 mm from the burner. In both cases: experimental data from [8], CD + C_1 model results by the method of [11,12], CD + ILDM model results from [5,6].

Fig. 6. Gauche : Profil de température moyenne conditionnelle à la distance axiale de 100 mm par rapport au brûleur. Droite : Profil de fraction massique moyenne en CO conditionnelle à la distance axiale de 150 mm par rapport au brûleur. Pour les deux cas, les données expérimentales sont celles publiées par [8], la méthode CD + C_1 est présentée par [11,12], les résultats de la méthode CD + ILDM sont ceux de [5,6].

ing model. A known deficiency of the CD model is that it is possible that particles reach a composition which is outside the stoichiometric region but in reality cannot be reached without passing the stoichiometric region. The model then predicts no ignition whereas in reality ignition would be expected. The scatter plot of the scalar PDF method with C_1-chemistry seems to show this effect. Less fully burnt conditions are observed than in the experiments.

It should be remarked that the different choice of model constant C_ϕ may also be relevant. In [12] the sensitivity with respect to the value of C_ϕ has been studied. It was concluded that with respect to conditional fluctuations, $C_\phi = 2$, seems the best value (provided an attached flame is predicted, i.e., at pilot flame power 300 W) and we have cited results for that value in this paper. In [5,6], however, a value of $C_\phi = 4$ was used, because in preliminary studies at $C_\phi = 2$ and $C_\phi = 3$ the flame did not attach to the burner. In [12] it was reported that lowering the value of C_ϕ leads to better predictions of mean temperature (provided the flame remains attached) at the cost of worse prediction of mixture fraction variance. It was also suggested that improving the model for Reynolds flux (e.g., by using the velocity-scalar PDF method), could lead to a simultaneous good prediction of both mean temperature and mixture fraction variance with a value of C_ϕ around the standard value $C_\phi = 2$. Such good prediction of both mixture fraction variance and mean temperature could not be realised in the calculations of [5,6] because at values of C_ϕ lower than 4 no attached flame was found. Further investigations are needed before conclusions can be drawn on the relative role of value of C_ϕ and model of the Reynolds flux.

To investigate the effects of micromixing and reaction in more detail we also looked at the CO mass fraction. Fig. 6 (right) shows the profile of conditional mean CO mass fraction at 150 mm. Fig. 7 shows the corresponding scatter plot of CO mass fraction versus mixture fraction. A drastic difference between the experiments and the two model predictions is observed. In the ILDM results almost no CO is seen at the rich side of the flame. This is a known deficiency of the first generation ILDM that has been used in [6,7]. At the rich side of the flame it is hard to describe the evolution in terms of only two reacting progress variables. The mathematical procedure of projection on the eigenspace belonging to the two slowest modes fails and is replaced by making an approximation to the manifold. Clearly this approximation is not sufficiently accurate for good prediction of CO mass fraction. In the recent literature alternatives for ILDM have been developed which can overcome this limitation [21,22]. The calculation with C_1-chemistry shows an overprediction of CO. It remains to be investigated to what extent this is due to the limitation of the chemistry scheme and the limitation of the CD micromixing model. The fact that differential diffusion is not taken into account in the micromixing model may play a role.

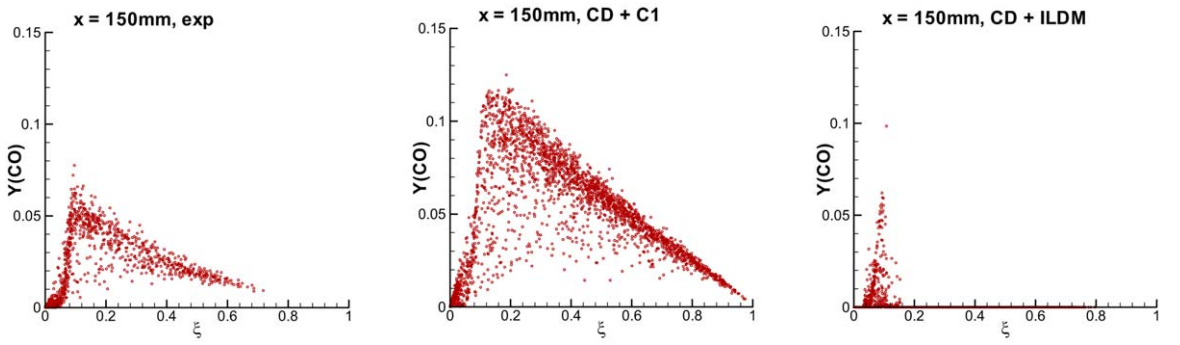

Fig. 7. Scatter plot of CO mass fraction versus temperature at axial distance 150 mm from the burner. Experimental data from [8], CD + C_1 model results by the method of [11,12], CD + ILDM model results from [5,6].

Fig. 7. Données de fraction massique en CO en fonction de la température à la distance axiale de 150 mm par rapport au brûleur. Les données expérimentales sont celles publiées par [8], la méthode CD + C_1 est présentée par [11,12], les résultats de la méthode CD + ILDM sont ceux de [5,6].

4. Conclusions and perspectives

A comparative analysis has been made of model predictions using Monte Carlo PDF methods for Delft Flame III. The flow field is well predicted (due to the quality of the turbulence model and the inlet boundary conditions). This is reflected in accurate radial profiles for mean velocity and mean mixture fraction. The reasons for the significantly better prediction of the mean temperature field in the scalar PDF calculations of [12] relative to the velocity-scalar PDF calculations of Refs. [6,7] has been discussed. It has been attributed to the impact of a better pilot flame model in combination with limitations of the CD micromixing model. A more detailed analysis should also take into account the dependence of the quality of mixture fraction variance prediction on the models for scalar dissipation rate and Reynolds flux. This would show the relative role of C_ϕ-value and Reynolds flux model. None of the models used gave a satisfactory prediction of the CO mass fraction. To make further progress with the analysis of this flame future work should elaborate the pilot flame model of [11,12], and increase the quality of the chemistry model employed. Only then strong conclusions on the relative performance of micromixing models for the Delft Flame III can be made.

Acknowledgements

The second author is Postdoctoral Fellow of the Fund of Scientific Research—Flanders (Belgium) (FWO-Vlaanderen). Part of the research was funded by FWO-Vlaanderen project G.0070.03. This work was done also as contribution to INTAS project 2000-353.

References

[1] S.B. Pope, PDF methods for turbulent reactive flows, Progr. Energy Combust. Sci. 11 (1985) 119–192.
[2] R.O. Fox, Computational Models for Turbulent Reacting Flows, Cambridge Univ. Press, 2003.
[3] S. Heinz, Statistical Mechanics of Turbulent Flows, Springer-Verlag, Berlin, 2003.
[4] R. Borghi, Turbulent combustion modelling, Progr. Energy Combust. Sci. 14 (1988) 245–292.
[5] P.A. Nooren, H.A. Wouters, T.W.J. Peeters, D. Roekaerts, U. Maas, D. Schmidt, Combust. Theory Model. 1 (1997) 79–96.
[6] P.A. Nooren, Stochastic modeling of turbulent natural-gas diffusion flames, PhD Thesis, Delft University of Technology, 1998.
[7] T.W.J. Peeters, P.P.J. Stroomer, J.E. de Vries, D.J.E.M. Roekaerts, C.J. Hoogendoorn, Proc. Combust. Inst. 25 (1994) 1241–1248.
[8] P.A. Nooren, M. Versluis, Th.H. van der Meer, R.S. Barlow, J.H. Frank, Appl. Phys. B 71 (2000) 95–111.
[9] E.H. van Veen, D. Roekaerts, On the accuracy of temperature measurements in turbulent jet diffusion flames by coherent Anti-Stokes Raman spectroscopy, Combust. Sci. Technol. 175 (2003) 1893–1914.
[10] http://www.ca.sandia.gov/TNF.
[11] B. Merci, B. Naud, D. Roekaerts, Flow and mixing fields for transported scalar PDF simulations of a piloted jet diffusion flame ('Delft Flame III'), Flow Turbulence Combust. 74 (2005) 239–272.
[12] B. Merci, D. Roekaerts, B. Naud, Study of the performance of three micro-mixing models in transported scalar PDF simulations of a piloted jet diffusion flame ('Delft Flame III'), Combust. Flame 144 (2006) 476–493.

[13] H.A. Wouters, T.W.J. Peeters, D. Roekaerts, Joint velocity-scalar PDF methods, in: B. Launder, N. Sandham (Eds.), Closure Strategies for Turbulent and Transitional Flows, Cambridge Univ. Press, 2002, pp. 626–655 (Chapter 22).
[14] B. Merci, E. Dick, Flow Turbulence Combust. 68 (2002) 335–358.
[15] B. Merci, E. Dick, C. De Langhe, Combust. Flame 131 (2002) 465–468.
[16] B. Merci, E. Dick, Int. J. Heat Mass Transfer 46 (2003) 469–480.
[17] S.M. Correa, Combust. Flame 93 (1993) 41–60.
[18] W.P. Jones, The joint scalar probability density function method, in: B. Launder, N. Sandham (Eds.), Closure Strategies for Turbulent and Transitional Flows, Cambridge Univ. Press, 2002, pp. 522–581 (Chapter 20).
[19] D. Roekaerts, Reacting flows and probability density function methods, in: B. Launder, N. Sandham (Eds.), Closure Strategies for Turbulent and Transitional Flows, Cambridge Univ. Press, 2002, pp. 328–337 (Chapter 10).
[20] P.P.J. Stroomer, Turbulence and OH structures in flames, PhD Thesis, Delft University of Technology, 1995.
[21] O. Gicquel, N. Darabiha, D. Thévenin, Laminar premixed hydrogen/air counterflow flame simulations using flame prolongation of ILDM with differential diffusion, Proc. Combust. Inst. 28 (2000) 1901–1908.
[22] J.A. van Oijen, L.P.H. de Goey, Modelling of premixed counterflow flames using the flamelet-generated manifold technique, Combust. Theory Model. 6 (2002) 463–478.